

Alpine Space report on projected future changes in weather extremes

X-RISK-CC

How to adapt to changing weather eXtremes and associated compound and cascading RISKs in the context of Climate Change



Contents

1	Introduction	2
2	Data	3
3	Methods.....	4
3.1	Climate index calculation	4
3.2	Global Warming Level aggregations and change patterns	5
3.3	Ensemble statistics.....	7
3.4	Analysis of changes under different Global Warming Levels	7
3.4.1	<i>Significant change patterns</i>	7
3.4.2	<i>Area percentage of significant changes</i>	8
4	Results.....	8
4.1.1	<i>Precipitation extremes</i>	8
4.1.2	<i>Wind extremes</i>	10
4.1.3	<i>Compound precipitation and wind extremes</i>	11
4.1.4	<i>Drought</i>	13
4.1.5	<i>Heat extremes</i>	15
4.1.6	<i>Compound drought and heat extremes</i>	16
5	Conclusions	18
6	References	18



1 Introduction

This report synthesizes the analyses carried out in the X-RISK-CC project for the detection and assessment of patterns and trends of past and future key weather extremes in the Alpine region. It complements the information displayed in the X-RISK-CC WebGIS and the local analyses carried out in the pilot areas and described in the pilot reports included in the Digital Library.

Based on in-depth analyses conducted in pilot areas, a set of 20 climate indices covering all relevant key weather extremes is calculated across the Alpine Space (AS) based on CERRA/CERRA-Land (Ridal et al., 2024) and ERA5 (Hersbach et al., 2020) reanalysis data and climate model projections (EURO-CORDEX, Jacob et al., 2014). The indices include information on extreme precipitation, wind speed, heat, drought and compound processes. Future changes in climate indices are assessed for different Global Warming Levels (GWLs) and aggregated model ensemble statistics. The synthesized high-level information about current and future extremes across AS are made available for visualization in the X-RISK-CC WebGIS. In the following, the most relevant change patterns based on GWLs are analyzed to investigate projected changes in intensity, frequency, spatial extent, and their uncertainty level.

2 Data

Reanalysis data from CERRA/CERRA-Land and ERA5 were used to describe current climate, while future projections were derived from EURO-CORDEX simulations (Table 1). The input variables needed for the calculation of climate indices were daily resolved precipitation totals, 10-meter maximum wind speed, 2-meter maximum and minimum temperature. Only EURO-CORDEX simulations providing the full set of required input variables were selected. All data has been reprojected to the same AS projection (EPSG:32632). Climate indices have been derived at annual and/or seasonal temporal aggregation and then aggregated over the periods corresponding to Global Warming Levels. All details about the data preprocessing can be found in the *About the Data* section of the X-RISK-CC WebGIS.

Table 1: EURO-CORDEX data selected for the calculation of AS climate indices.

Regional Climate Model (RCM)	Global Climate Model (GCM)	Ensemble Member
COSMO-crCLIM-v1-1	CNRM-CM5	r1i1p1
COSMO-crCLIM-v1-1	EC-EARTH	r1i1p1
COSMO-crCLIM-v1-1	EC-EARTH	r3i1p1
COSMO-crCLIM-v1-1	EC-EARTH	r12i1p1
COSMO-crCLIM-v1-1	HadGEM2-ES	r1i1p1
COSMO-crCLIM-v1-1	MPI-ESM-LR	r1i1p1
COSMO-crCLIM-v1-1	MPI-ESM-LR	r2i1p1
COSMO-crCLIM-v1-1	MPI-ESM-LR	r3i1p1
COSMO-crCLIM-v1-1	NorESM1-M	r1i1p1
RCA4	CNRM-CM5	r1i1p1



RCA4	EC-EARTH	r1i1p1
RCA4	EC-EARTH	r3i1p1
RCA4	EC-EARTH	r12i1p1
RCA4	HadGEM2-ES	r1i1p1
RCA4	MPI-ESM-LR	r1i1p1
RCA4	MPI-ESM-LR	r2i1p1
RCA4	MPI-ESM-LR	r3i1p1
RCA4	IPSL-CM5A-MR	r1i1p1
RCA4	NorESM1-M	r1i1p1

3 Methods

3.1 Climate index calculation

Table 2 lists all calculated climate indices and their use cases described by keywords. In total, 20 climate indices are calculated and cover extreme precipitation, wind, heat and drought, as well as compound extremes of precipitation and wind and heat and drought. This enables broad analyses covering different types of natural hazards. More details on the index calculation and definitions are provided in the *About the Data* section of the WebGIS and in *WebGIS index description* document in the Digital Library.

Climate indices are calculated using xarray (<https://pypi.org/project/xarray/>) and methods built thereupon, as well as using xclim. All climate indices are calculated for both seasonal and annual temporal aggregation. Exceptions to this are the heat-related indices and the two convective indicators, which are only calculated on an annual basis. All indices are then further aggregated to Global Warming Levels (see next section).

Table 2: Overview of all calculated climate indices for the Alpine Space and their use case.

Climate index name	Abbreviation	Use case
Maximum 1-day precipitation	Rx1d	Extreme 1-day precipitation intensity
Maximum 3-day precipitation	Rx3d	Extreme multi-day precipitation intensity
Number of days with 1-day precipitation exceeding the 97 th percentile	R97pN_1d	Extreme 1-day precipitation frequency
Sum of 1-day precipitation exceeding the 97 th percentile	R97pTOT_1d	Extreme 1-day precipitation cumulative intensity
Number of days with 3-day precipitation exceeding the 97 th percentile	R97pN_3d	Extreme multi-day precipitation frequency
Sum of 3-day precipitation exceeding the 97 th percentile	R97pTOT_3d	Extreme multi-day precipitation cumulative



		intensity
Convective indicator orange warning	conv_ind_orange	Extreme convective precipitation
Convective indicator red warning	conv_ind_red	Very extreme convective precipitation
Maximum 1-day wind speed	WSx1d	Extreme wind speed intensity
Number of days with 1-day wind speed exceeding the 97 th percentile	WS97pN_1d	Extreme wind speed frequency
Mean of maximum wind speed for days exceeding the 97 th percentile	WS97pMEAN_1d	Wind speed on very windy days
Number of days with extreme 3-day precipitation and 1-day wind speed maximum	RWS97pN_3d	Compound extreme precipitation and wind frequency
One-month drought peak intensity	SPEI1_int	Peak intensity of one-month drought
One-month drought frequency	SPEI1_freq	Frequency of one-month severe drought conditions
Three-month drought peak intensity	SPEI3_int	Peak intensity of three-month drought
Three-month drought frequency	SPEI3_freq	Frequency of three-month severe drought conditions
Heatwave days	HWD	Heatwave frequency
Heatwave magnitude	HWM	Heatwave intensity
Magnitude of compound one-month drought and heatwave events	CDHW_1	Compound heatwave and one-month drought magnitude
Magnitude of compound three-month drought and heatwave events	CDHW_3	Compound heatwave and three-month drought magnitude

3.2 Global Warming Level aggregations and change patterns

The current climate conditions are derived from reanalysis data by averaging the indices over the 1991-2020 period. To derive the changes under different magnitudes of warming, aggregations to Global Warming Levels (GWLs) are adopted. GWLs are intended to represent the expected climate conditions under different magnitudes of global temperature increases (e.g., +2 °C, +3 °C) with respect to the pre-industrial period (1850-1900). We use the derived GWLs based on the Intergovernmental Panel on Climate Change (IPCC) methodology (Hauser et al., 2022). However, since those are based on 20-year periods and for all previous analyses 30-year periods have been used, we prolong the IPCC GWL periods by 5-years in each direction, thereby covering 30-years, while keeping the center of the period unchanged. The used GWLs for each model are listed in Table 3. It is worth noticing that GWLs cannot be directly associated to a well-defined future period since it varies with models. However, the higher the warming level is, the later it is reached into



the future (Figure 1). For each model simulation, all climate indices at their annual/seasonal temporal resolution are averaged across time within the corresponding GWL period, yielding one value for each grid cell and GWL. The historical reference period used to calculate the projected changes for each considered GWL (i.e., +1.5, +2, +3, +4 °C) is derived based on the Global Warming Level +1 °C which roughly coincides with the 1991-2020 period (Figure 1).

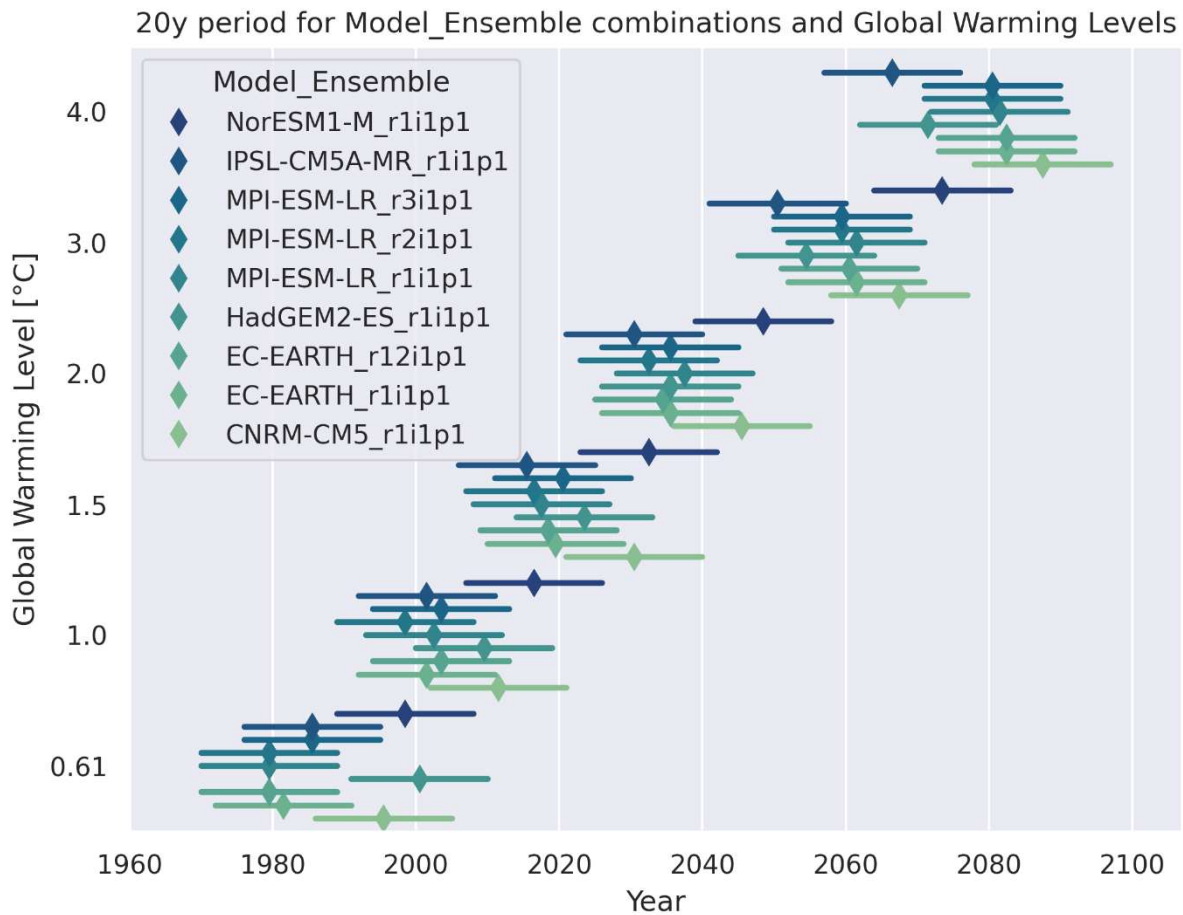


Figure 1: Time periods (start, central and end year) for different Global Warming Levels for the driving GCMs of the used EURO-CORDEX simulations.

Table 3: Global Warming Levels for the driving GCMs of the used EURO-CORDEX simulations, extended to 30-year periods. Model-GWL combinations without available GWLs are marked with "-" and are not used for the analyses on the specific GWL

GCM	Ensemble Member	GWL 1°C	GWL 1.5 °C	GWL 2 °C	GWL 3 °C	GWL 4 °C
CNRM-CM5	r1i1p1	1997-2026	2016-2045	2031-2060	2053-2082	2073-2102
EC-EARTH	r1i1p1	1987-2016	2005-2034	2021-2050	2047-2076	2068-2097
EC-EARTH	r3i1p1	-	-	-	-	-
EC-EARTH	r12i1p1	1989-2018	2004-2033	2020-2049	2046-2075	2068-2097
HadGEM2-ES	r1i1p1	1995-2024	2009-2038	2021-2050	2040-2069	2057-2086



MPI-ESM-LR	r1i1p1	1988-2017	2003-2032	2023-2052	2047-2076	2067-2096
MPI-ESM-LR	r2i1p1	1984-2013	2002-2031	2018-2047	2045-2074	2066-2095
MPI-ESM-LR	r3i1p1	1989-2018	2006-2035	2021-2050	2045-2074	2066-2095
NorESM1-M	r1i1p1	2002-2031	2018-2047	2034-2063	2059-2088	-
IPSL-CM5A-MR	r1i1p1	1987-2016	2001-2030	2016-2045	2036-2065	2052-2081

To analyze changes for different levels of warming, the spatial patterns for different GWLs are simply subtracted, e.g., $\Delta GWL(4\text{ }^{\circ}\text{C}) = GWL(4\text{ }^{\circ}\text{C}) - GWL(1\text{ }^{\circ}\text{C})$ is the change pattern for GWL 4 °C. The change patterns with respect to the present state of the climate are derived by comparing the future GWLs with GWL +1 °C instead of with reanalysis fields directly. It is meant to remove the influence of potential biases in climate model simulations with respect to reanalysis data, which might affect the result accuracy.

3.3 Ensemble statistics

To reduce the overall complexity and dimensionality of the data, all calculated climate indices for each GWL are further reduced by calculating ensemble statistics across all models. Specifically, the 5th, 25th, 50th, 75th and 95th percentiles of the model ensemble are calculated for each grid cell, index, GWL and annual/seasonal aggregation. The resulting maps of ensemble statistics are used to analyse the spatial patterns of projected changes as well as the variability range for each index and can be conveniently displayed in the WebGIS. All WebGIS data are also accessible through the Zenodo repository (<https://doi.org/10.5281/zenodo.14704314>).

3.4 Analysis of changes under different Global Warming Levels

A brief synthesis of projected changes in extreme weather indices across the AS is given in the result section. For this, we mainly focus on the GWL +3 °C as one of the most realistic scenarios targeting the middle of the century. Annually aggregated climate indices are primarily discussed, although information for other GWLs and seasonally aggregated indices is provided whenever meaningful. The following metrics are considered:

- Change pattern of the ensemble median, supported by the significance of changes;
- Area percentage of significant changes per GWL.

3.4.1 Significant change patterns

The change patterns focus on the median of the model ensemble, instead of higher or lower percentiles, for a more robust and plausible analysis of how the future may look like. The significance is evaluated based on two criteria: (i) 80% agreement across the ensemble in terms of the direction of change (positive/negative), and (ii) significance in terms of a Mann-Whitney-U test (MWUt) between the ensemble values of GWL +1 °C and the GWL in question. Changes are considered significant when both criteria are fulfilled, that is, when at least 80% of the ensemble agree in the direction of change and the p-value from the MWUt is below 0.05. This follows the IPCC in terms of outlining robust and significant changes (IPCC, Masson-Delmotte, et al., 2021). Significant changes are visualized in the maps provided in the following with a lack of hatching, while all non-significant areas are hatched.

The change pattern for the ensemble median of annual Rx3d for GWL +4 °C is shown in Figure 2 as an example. A more comprehensive analysis is given in the next section.



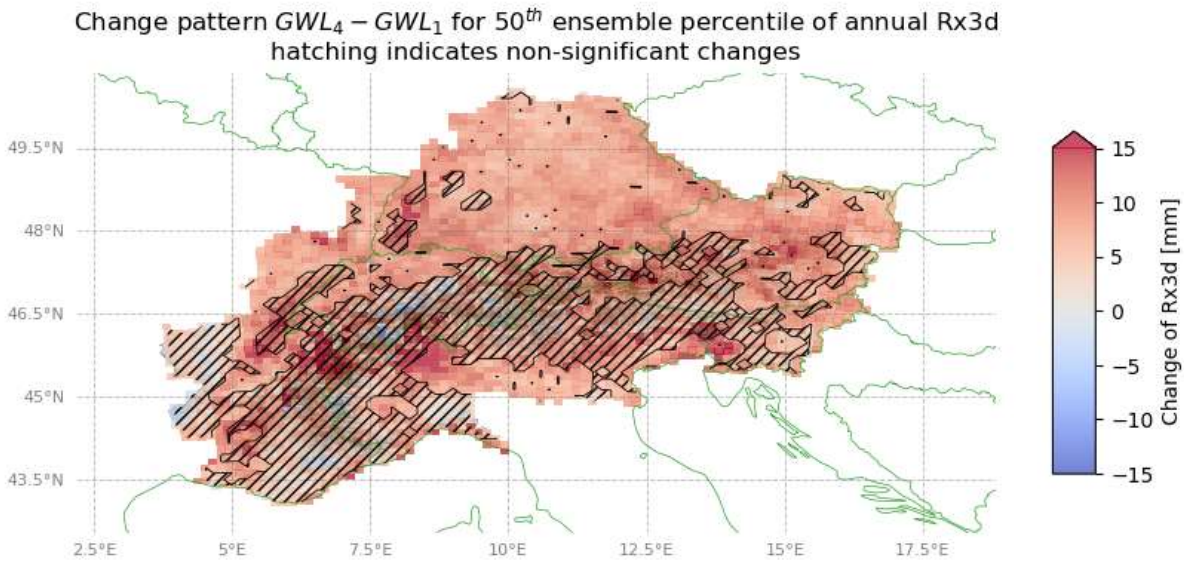


Figure 2: Change pattern for the ensemble median of annual Rx3d for the +4 °C global warming level. While increases in Rx3d are prevalent overall and more pronounced, indicating increased intensity of multi-day precipitation, there are also some smaller regions that show a slight decrease. However, projected changes in all the regions showing a decline as well as in most regions south of the main Alpine ridge are not significant (hatching).

3.4.2 Area percentage of significant changes

The area percentage of significant changes is simply the portion of grid cells that show significant changes divided by the total number of grid points in the AS area. Additionally, the significant changes are derived for positive (increasing) and negative (decreasing) changes, separately. For each climate index, the resulting areal portion of significant changes over increasing GWLs is analyzed.

4 Results

In this subsection, the results for the analysis of possible future changes for different meteorological categories covered by the climate indices are shown and discussed.

4.1.1 Precipitation extremes

Both Rx1d and Rx3d show increases for the GWL +3 °C and the ensemble median for most AS, with Rx3d additionally exhibiting some decreases in the Po valley and the Italian-Swiss border region. However, most of the changes especially in the southern Alpine region is not significant. The major significant changes are increases in both quantities in the northern and north-eastern parts of the Alpine space domain. Hence, the changes in annual day to multi-day intensity maxima are not fully conclusive but show an increasing tendency overall. For R97pN_1d, R97pTOT_1d and R97pN_3d, R97pTOT_3d the changes are more conclusive, showing significant increases in most of the domain (Figure 3). The exception is northern Italy and the South-West of the domain, which is not significant due to the changes being not as pronounced compared to the rest of the area. Finally, the projected changes for the convective indicator are more relevant under GWL +4 °C and suggest a widespread increase in extreme thunderstorm probability although the changes are not significant for the most part. The inner Alpine ridge is the only area where the intensification of convective phenomena is significant and shows the strongest increases (Figure 4). Figure 5 reports the portion of the Alpine Space affected by significant changes in R97pN_3d with increasing GWLs. The pattern is mostly similar



among the precipitation-related indices, which shows that the area affected by significant changes is limited for GWLs +1.5 and +2 °C, but it exceeds 50% of the domain for GWL +3 and +4 °C with statistically significant increases. Overall, while the exact change for extreme precipitation depends on the index, there is a clear tendency for more intense precipitation and more concentrated extreme precipitation days in many regions across the Alpine Space and a clear relationship between increasing GWLs and more intense and widespread changes.

Change pattern $GWL_3 - GWL_1$ for 50th ensemble percentile of annual R97pN_1d
hatching indicates non-significant changes

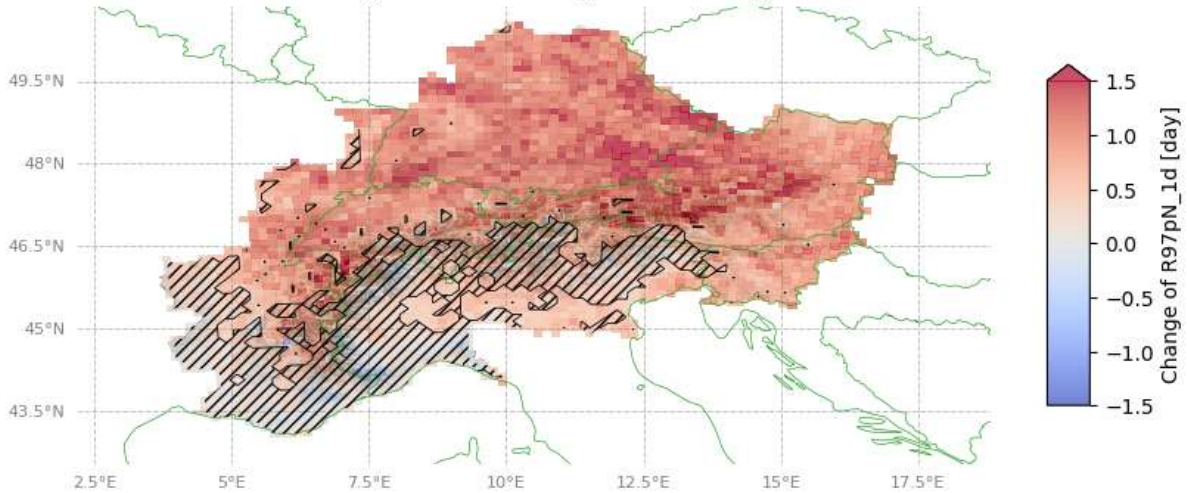


Figure 3: Change pattern of R97pN_1d for GWL +3 °C, showing a statistically significant increase in most of the domain, with the exceptions being northern Italy and the south-western Alps.

Change pattern $GWL_4 - GWL_1$ for 50th ensemble percentile of annual conv_ind_red
hatching indicates non-significant changes

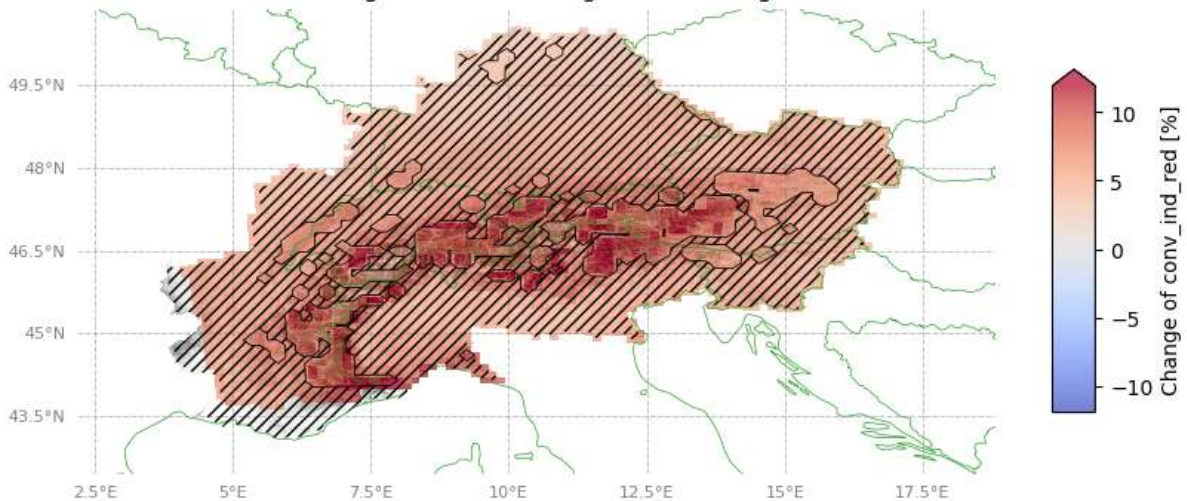


Figure 4: Change pattern of the convective indicator for red-warning thunderstorms for GWL +4 °C. The changes are most pronounced and statistically significant along the Alpine ridge. Lower GWLs indicate less pronounced intensification.



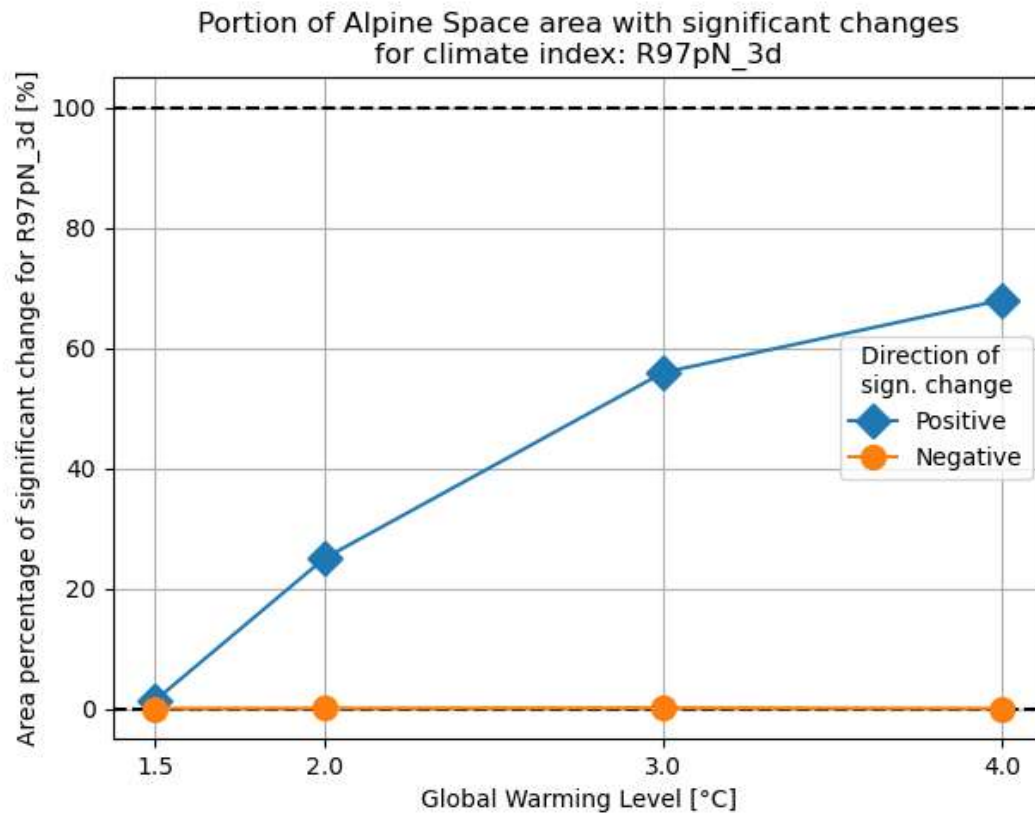


Figure 5: Percentage of AS area affected by significant changes for R97pN_3d. Most of the precipitation-related indices share a similar pattern, namely that the area affected by significant changes is limited for GWLs +1.5 and +2°C, but exceeds 50 % of the domain for GWL +3 and +4°C.

4.1.2 Wind extremes

The wind-related indices are used to evaluate changes in frequency and intensity of daily wind speed extremes. Both indices related to intensity, WS97pMEAN_1d and WSx1, show only relatively small and non-significant changes across the domain. There is a tendency for slightly more intense winds north of the Alps in southern Germany and less intense winds in northern Italy, but since the changes are not significant, the consensus remains inconclusive. For WS97pN_1d, some smaller regions of significant decreases in the annual frequency of days with extreme winds are visible in northern Italy (Figure 6), however, the magnitude of decreases remains limited, being only around one day. Figure 7 shows the portion of the area with significant changes for increasing GWLs. Evidently, there is no clear emerging trend between GWLs and areas reporting significant changes, however, the ensemble shows that some portion of the AS is projected to experience significant changes, which are mostly decreasing. Overall changes for wind extremes are therefore mostly inconclusive without significant changes in either direction, except for a tendency towards less extreme windy days in some parts of northern Italy.



Change pattern $GWL_3 - GWL_1$ for 50th ensemble percentile of annual WS97pN_1d hatching indicates non-significant changes

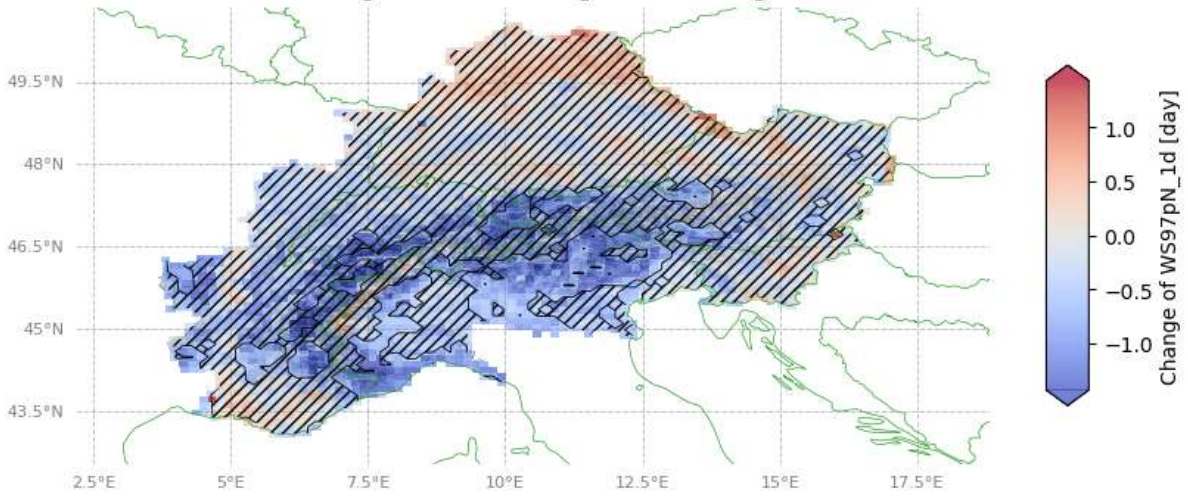


Figure 6: Change pattern of WS97pN_1d for $GWL +3\text{ }^\circ\text{C}$. While most of domain exhibits non-significant changes, a small statistically significant decrease is visible in northern Italy.

Portion of Alpine Space area with significant changes for climate index: WS97pN_1d

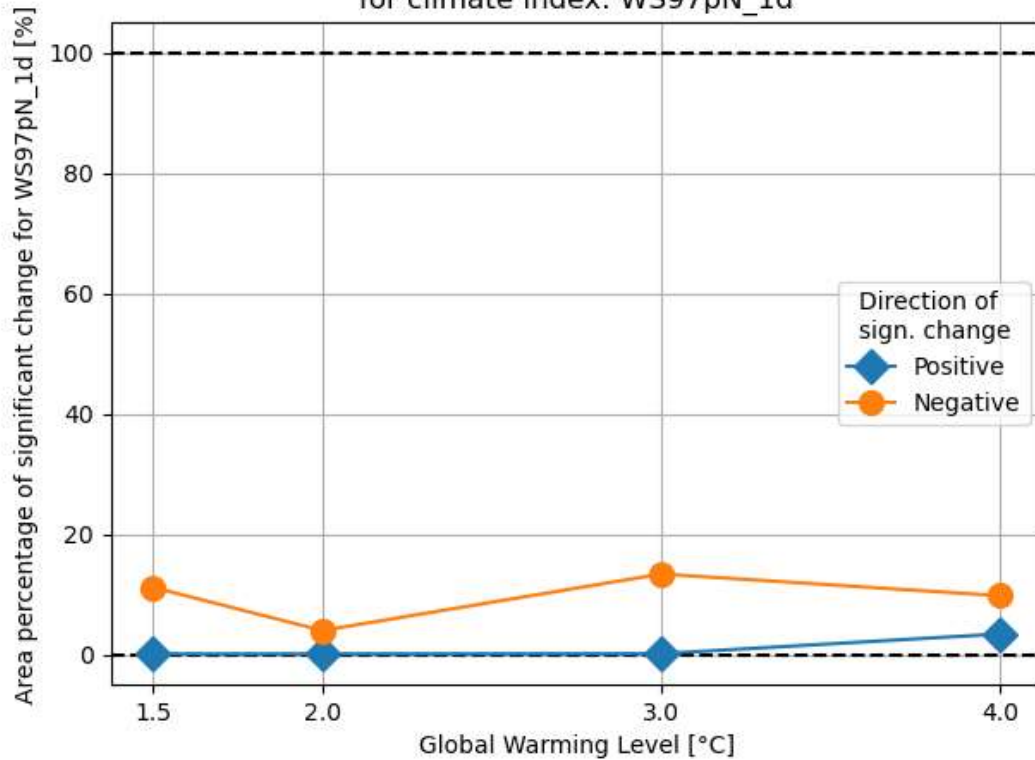


Figure 7: Percentage of AS area affected by significant changes in WS97p1N. The extent of significant changes shows no clear relationship to increasing GWLs.

4.1.3 Compound precipitation and wind extremes

The index for compound precipitation and wind extremes depicts changes in the frequency of days



when extreme precipitation and wind coincide. The change patterns for $GWL +3\text{ }^{\circ}\text{C}$ and for the area portion affected by significant changes are reported in Figure 8 and Figure 9, respectively. The main Alpine ridge shows a minor decrease in the frequency of compound events although it remains non-significant. Statistically significant changes are mainly visible in southern Germany. The portion of affected area shows a clear relationship between the increase in GWL and increase in the frequency of compound precipitation and wind extremes, which is driven by precipitation, as evident from the precipitation indices.

Change pattern $GWL_3 - GWL_1$ for 50th ensemble percentile of annual $RWS97pN_3d$
hatching indicates non-significant changes

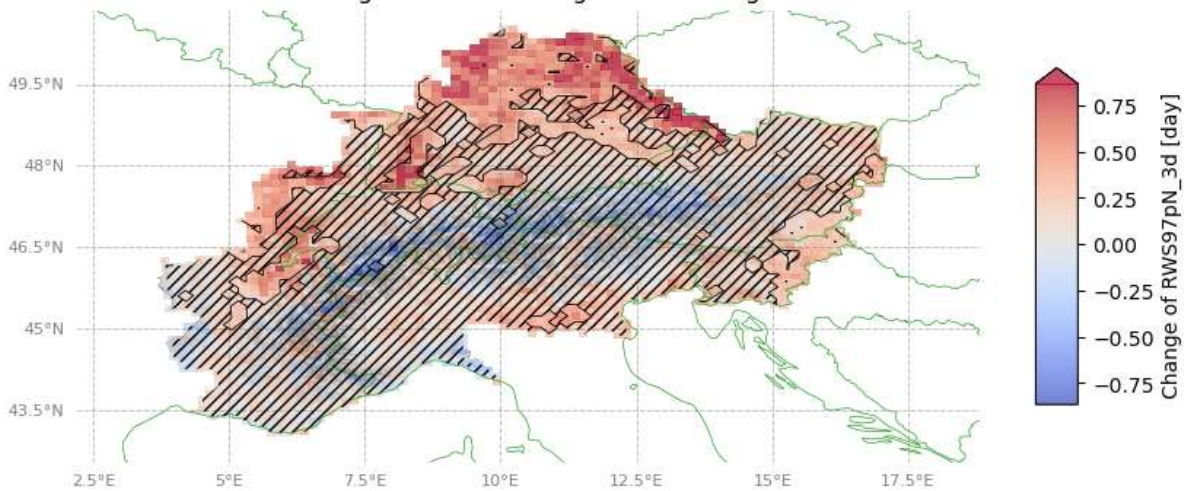


Figure 8: Change pattern of the compound index $RWS97pN_3d$ for $GWL +3\text{ }^{\circ}\text{C}$. Notably, while the main Alpine ridge shows a minor decrease, this change is not significant. Statistically significant increases are found mostly in southern Germany.



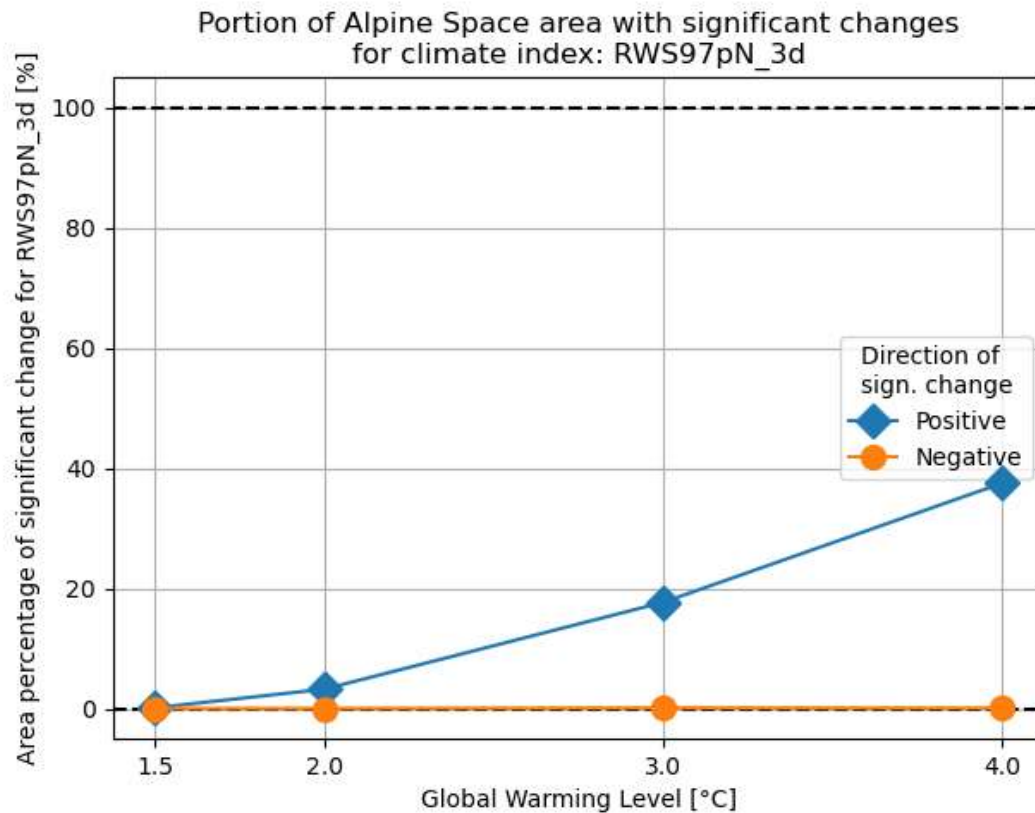


Figure 9: Percentage of AS area affected by significant change in the frequency of compound precipitation and wind extremes. It shows a clear increasing relationship with increasing GWLs.

4.1.4 Drought

Changes in drought conditions are depicted based on the peak intensity and frequency of low SPEI (Standardized Precipitation and Evapotranspiration Index) values over one- and three-month-time windows. Figure 10 shows a clear picture of intensification for drought events via the decrease of SPEI1_int (and SPEI3_int, not shown), while also being statistically significant in most of the domain. The most pronounced intensification of drought conditions is detected in the south-western portion of the AS. While for SPEI1_int the non-significant areas of change are mostly limited to some smaller regions of north-western and north-eastern Austria, for SPEI3_int the non-significant area extends across northern Austria and south-eastern Germany. SPEI1_freq and SPEI3_freq (not shown) show similar change patterns across the domain, with the greatest increases in drought frequency in the south-western Alps. The percentage of area with significant changes for increasing GWLs shows consistent behavior across all drought indices (Figure 11). For GWL +1.5 and +2 °C, about 40% of the area is affected by significant decreases of SPEI1_int (which equals an increase of drought peak intensity), whereas, for GWL +3 and +4 °C, more than 90% of AS is projected to experience significant changes in drought conditions. It is worth noting that indices based on one-month drought conditions exhibit wider areas affected by significant changes compared to the indices considering three-month drought, but with the same characteristics.



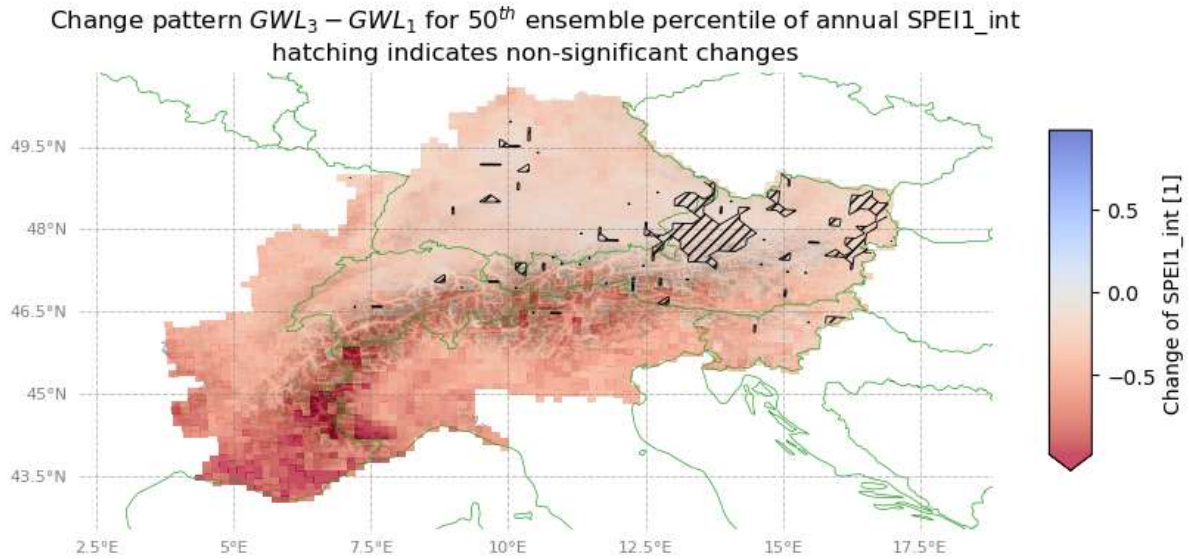


Figure 10: Change pattern of SPEI1_int for $GWL +3\text{ }^\circ\text{C}$. SPEI1_int shows an overall increase in the peak intensity of one-month drought conditions (more negative SPEI1_int values). Additionally, this change is almost everywhere statistically significant. The south-western Alps show more intensifying droughts compared to the rest of the domain.

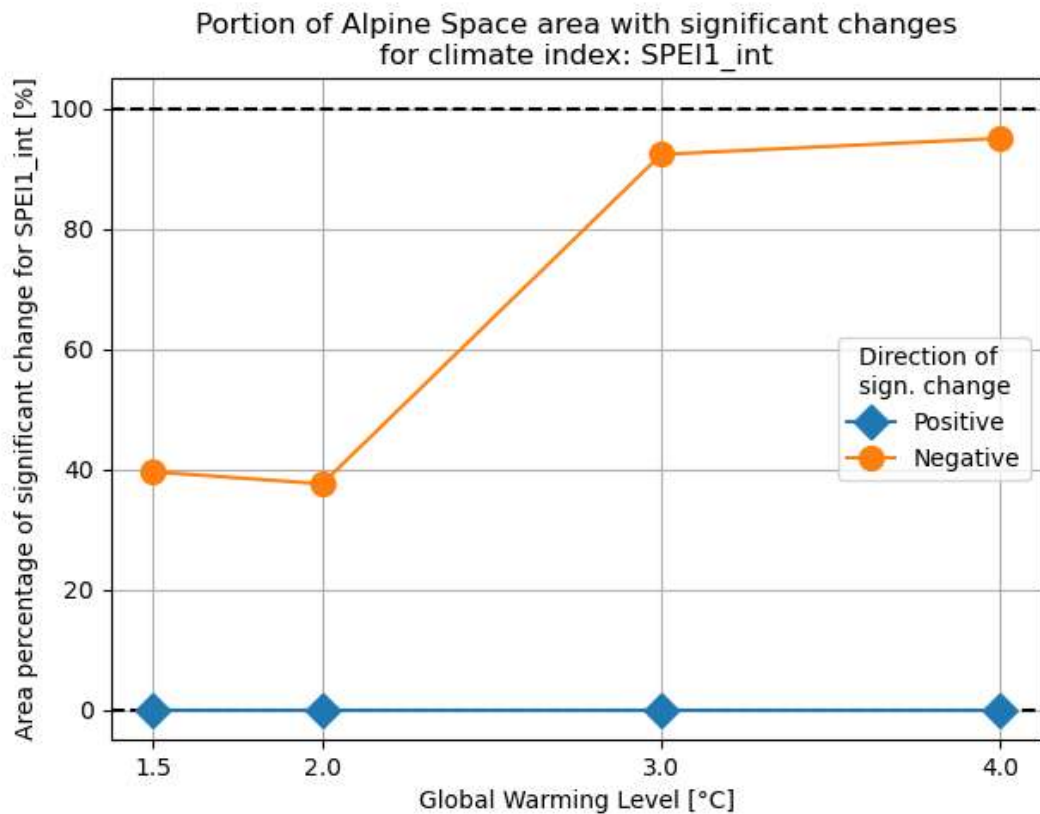


Figure 11: Percentage of the AS area affected by significant change for SPEI1_int. A distinct pattern is detected: a smaller portion of the area report significant changes for $GWL +1.5$ and $+2\text{ }^\circ\text{C}$, while it increases substantially for $GWL +3$ and $+4\text{ }^\circ\text{C}$.



4.1.5 Heat extremes

Heat extremes are depicted via HWM and HWD, describing changes in the magnitude and frequency of heatwave periods, respectively. Figure 12 shows the changes in HWD for $GWL +3\text{ }^{\circ}\text{C}$, exhibiting statistically significant increases in the frequency of days experiencing extreme heat conditions throughout the Alpine Space. The changes for HWM (not shown) are similarly striking, showing an overall intensification of heatwaves. Figure 13 clearly shows that even for the lower $GWL (+1.5\text{ }^{\circ}\text{C})$, practically all AS is affected by statistically significant increases.

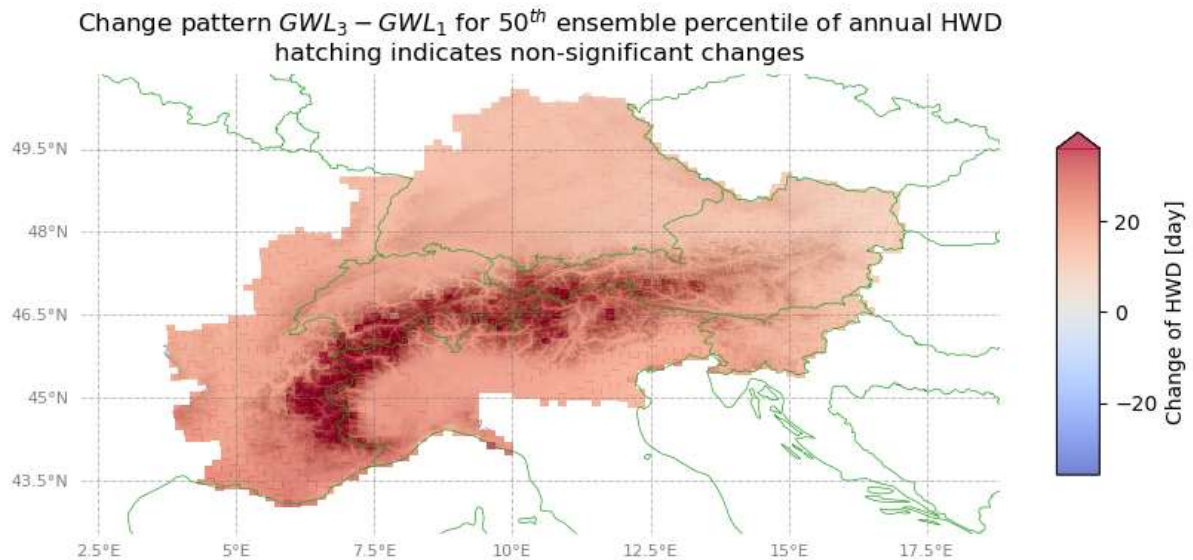


Figure 12: Change pattern of heatwave days (HWD) for $GWL +3\text{ }^{\circ}\text{C}$. Statistically significant increases are evident across all the domain, upwards of 30 extra heatwave days for parts of the Alpine ridge with respect to current conditions.



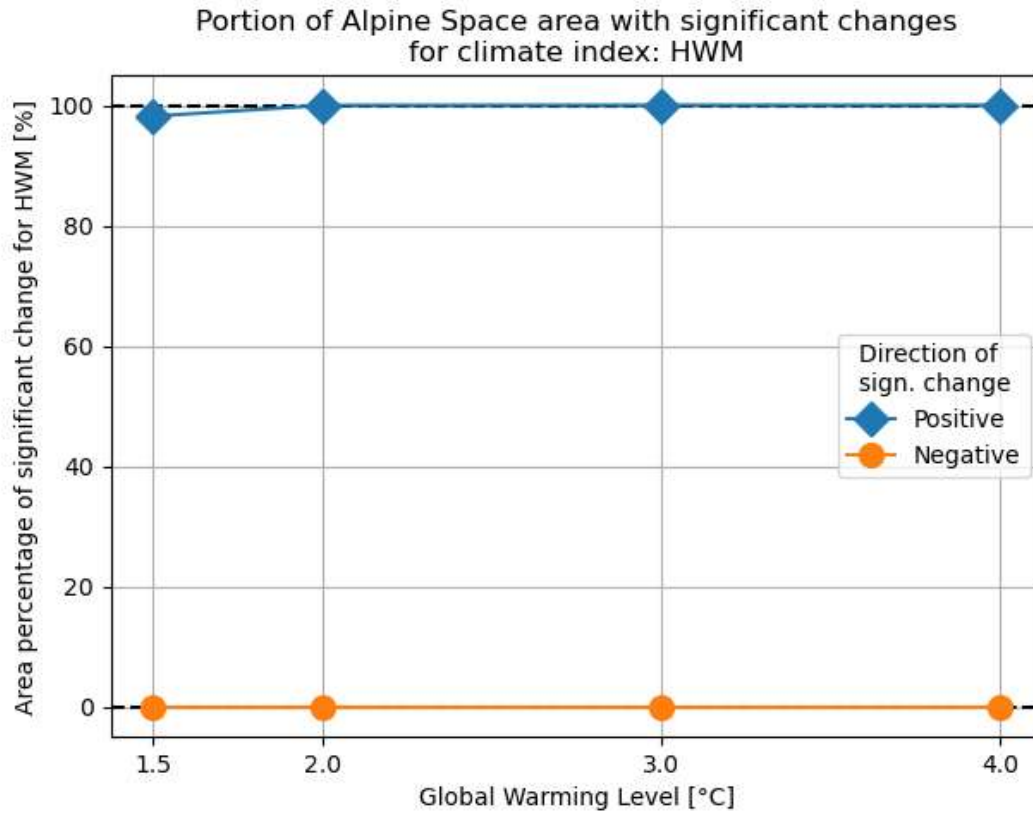


Figure 13: Percentage of AS area affected by significant changes for HWM. Significant changes are projected everywhere for all GWLs, with the slight exception of a few grid cells for GWL +1.5 °C.

4.1.6 Compound drought and heat extremes

Changes for compound drought and heat extremes follow the patterns shown above for individual extremes and depict an overall intensification of the phenomena. Figure 14 depicts significant changes in the magnitude of compound heatwave and one-month drought events (CDHW_1) across the domain with the greatest intensification in the south-western Alps. Similar patterns are obtained by considering the magnitude of compound heatwave and three-month drought events (CDHW_3). The variation in the area affected by significant changes (Figure 15) is driven by the pattern of drought-related indices (Figure 13): for GWL +1.5 and 2 °C around half of the domain reports significant positive changes, while for GWL +3 and +4 °C all of the Alpine Space is projected to experience statistically significant increases in the magnitude of compound drought and heat extreme events.



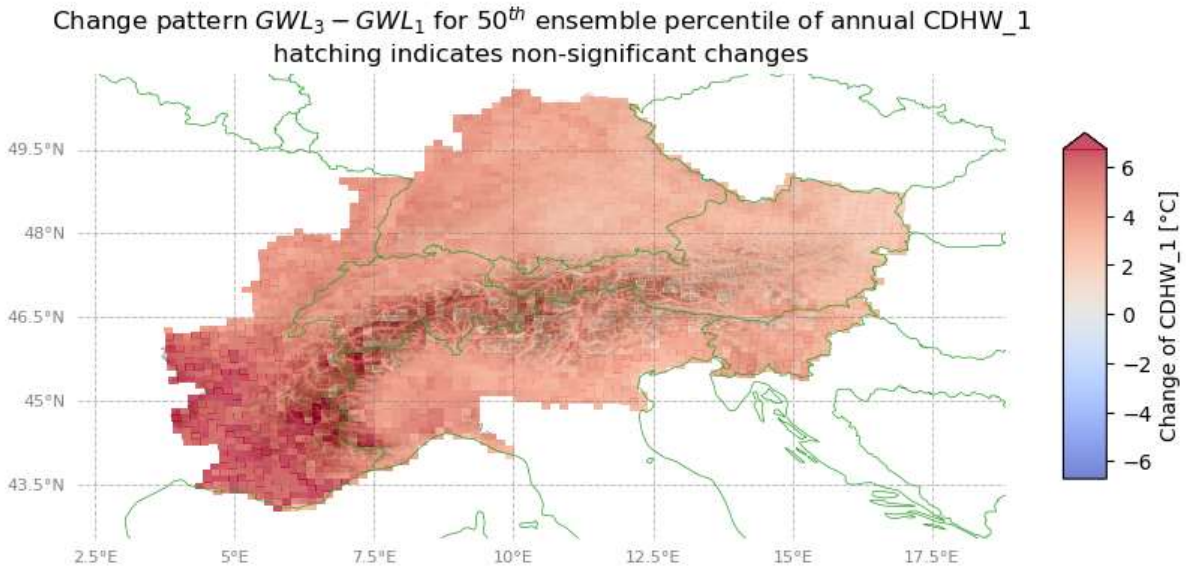


Figure 14: Change pattern of compound drought-heat magnitude for $GWL +3$ °C. It shows statistically significant increases throughout the Alpine Space with the most intensification in the south-western Alps.

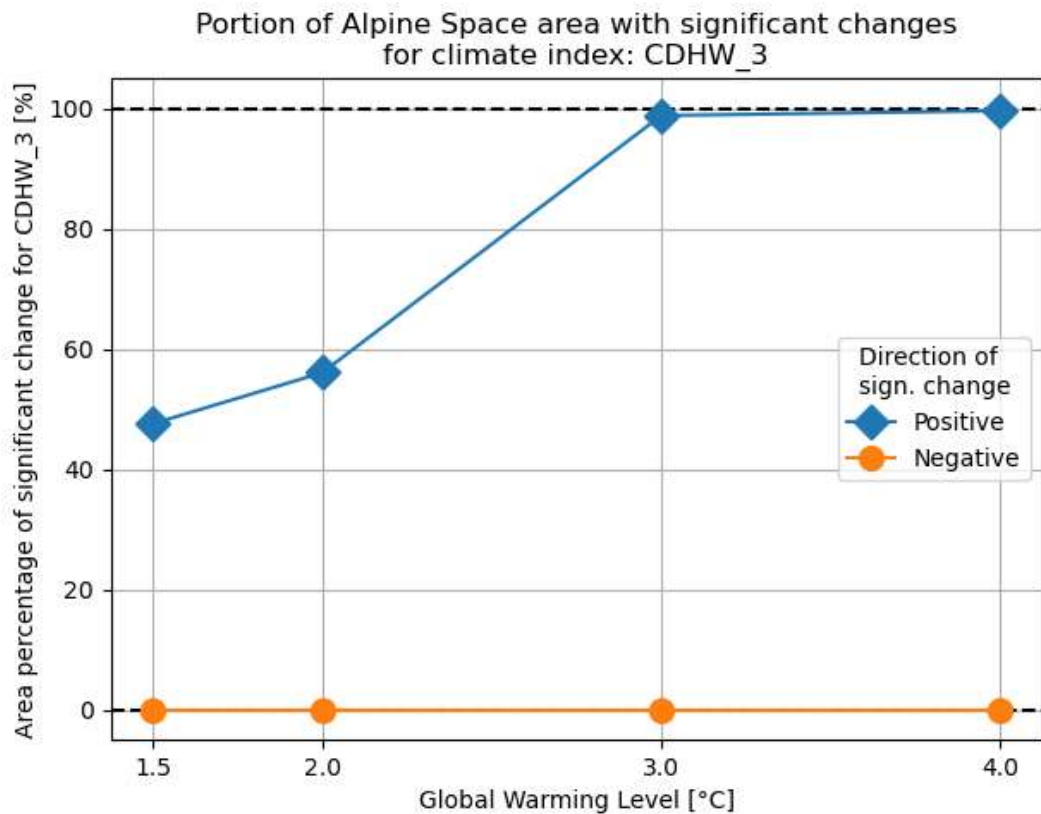


Figure 15: The percentage of area affected by significant changes of CDHW_3. It follows the pattern from drought-related indices, wherein $GWL +1.5$ and $+2$ °C show roughly half of the Alpine Space area experiencing significant changes, while for $GWL +3$ and $+4$ °C changes are significant throughout the domain.



5 Conclusions

The Alpine Space is projected to experience changes in extreme weather conditions, that vary depending on the weather phenomenon and the Global Warming Level considered. Drought, heat and compound drought-heat extremes are the processes showing the strongest intensification and frequency increase across the whole domain and across all GWLs analyzed, while being more pronounced with higher GWLs. A spatial hotspot in terms of changes for these phenomena is the south-western Alps, which exhibit the largest changes for several indices. The picture for precipitation is not as conclusive. The relationship between increasing 1-day and 3-day extreme precipitation intensity as well as frequency and increasing GWLs is clear, but the changes vary spatially. Generally, the region north of the Alpine ridge exhibits statistically significant increases in both intensity and frequency, while both increases and decreases are projected south of the Alpine ridge, but all of which being not statistically significant. The convective indicators, describing the probability for severe or extreme thunderstorms, show increases across the domain, however, only in some parts the increases are statistically significant and mostly only for the highest GWL +4 °C, particularly in north-eastern Italy and south-western Austria. Wind extremes are overall inconclusive, showing varying magnitude and direction of changes that are almost all not significant. The only exception is represented by the frequency of extreme wind occurrences in some regions of northern Italy, which shows statistically significant decreases. Similarly, no conclusive remarks can be derived for compound precipitation-wind extremes, stemming from the lack of significant changes from wind extremes. Albeit there is a relationship between an increasing area affected by significant changes with increasing GWLs, this area is limited to mostly southern Germany and south-eastern Austria.

6 References

Hersbach, H., Bell, B., Berrisford, P., et al. (2020). The ERA5 global reanalysis. *Q. J. R. Meteorol. Soc.*, 146, 1999–2049. <https://doi.org/10.1002/qj.3803>

Jacob, D., Petersen, J., Eggert, B., Alias, A., Christensen, O.B., Bouwer, L.M., Braun, A., Colette, A., Déqué, M., Georgievski, G. and Georgopoulou, E., (2014). EURO-CORDEX: new high-resolution climate change projections for European impact research, *Reg. Environ. Change*, 14, 563–578. <https://doi.org/10.1007/s10113-013-0499-2>

Masson-Delmotte, V., Zhai, P., Pirani, A., Connors, S.L., Péan, C., Berger, S., Caud, N., Chen, Y., Goldfarb, L., Gomis, M.I. and Huang, M., 2021. Climate change 2021: the physical science basis. Contribution of working group I to the sixth assessment report of the intergovernmental panel on climate change, 2(1), p.2391.

Ridal, M., Bazile, E., Le Moigne, P., Randriamampianina, R., Schimanke, S., Andrae, U., et al. (2024). CERRA, the Copernicus European Regional Reanalysis system, *Quarterly Journal of the Royal Meteorological Society*, 150(763), 3385–3411. <https://doi.org/10.1002/qj.4764>

